PHYSICAL REVIEW A VOLUME 22, NUMBER 3 SEPTEMBER 1980

Saturation of resonant third-harmonic generation in phase-matched systems

H. Puell,* H. Scheingraber, and C. R. Vidal
Max-Planck-Institut für Extraterrestrische Physik, 8046 Garching, München, Germany
(Received 4 February 1980)

The saturation of resonant third-harmonic generation in absorbing and phase-matched high-density systems is investigated theoretically as well as experimentally. It is shown that the saturation is determined by the two-photon absorption [imaginary part of $\chi_s^{(3)}(\omega)$]. It gives rise to a depletion of the fundamental wave and leads to a change of the level populations and of the effective refractive index destroying the phase matching. This has to be compared with nonresonant systems which are limited by the Kerr effect, the intensity-dependent changes of the refractive index [real part of $\chi_s^{(3)}(\omega)$]. Optimum conditions for resonant systems are reported.

I. INTRODUCTION

Since the first paper on resonant third-harmonic generation (THG) in Sr-vapor,[1] a large number of publications have dealt with the generation of coherent radiation in the vacuum ultraviolet spectral region. While the first experiments[1-6] were performed with nanosecond light pulses, the interest shifted to the application of picosecond pulses[7-10] since time-integrating effects like ionization losses were thought to be destructive to the process of harmonic generation. Recently, however, Scheingraber *et al.*[11] demonstrated that, even with flash-lamp-pumped dye lasers, conversion efficiencies in excess of 10^{-5} are feasible at moderate input intensities as low as 5×10^6 W/cm^2.

The resonantly enhanced polarization gives rise to appreciable conversion efficiencies at much lower input intensities than in nonresonant systems. At high input intensities, however, the resonant systems investigated so far show severe saturation which limits the maximum energy-conversion efficiency to less than 10^{-3}, which has to be compared with conversion efficiencies as high as 0.1 achieved in nonresonant systems.[12-13]

For nonresonant THG, saturation effects have recently been studied in detail by Puell and Vidal.[14] It was shown that the maximum attainable conversion depends only on the material parameters of the nonlinear medium, namely the ratio of the third-harmonic susceptibility $\chi_T^{(3)}$ and the Kerr constants $\chi_S^{(3)}$. The saturation is determined by the breakup of the phase-matching condition due to the intensity-dependent changes of the refractive indices.

For resonant THG, however, the results of Puell and Vidal[14] are no longer applicable, since the physical processes which lead to saturation, are more complicated because of the absorption processes involved. Furthermore, resonant systems are very sensitive to the time scale of the generating light pulse. For picosecond pulses, e.g., coherent excitations and their implications on the pulse propagation have to be considered.[15-17] In this paper, however, a discussion of the saturation phenomena observed with pulses of 600-nsec duration is given. In this time domain several attempts have been made to explain the saturation observed in the, so far, most carefully examined experiment on resonant THG by Ward and Smith[4]:

(i) Ward and Smith[4] interpreted their results on the basis of population saturation, where the resulting power-broadening of the resonant transition leads to a $P(3\omega)\propto P(\omega)^{-1}$ dependence for the generated harmonic power $P(3\omega)$ at large input powers $P(\omega)$.

(ii) Elgin and New[18] showed that the optical Stark shift, neglected by Ward and Smith, compensates the population saturation and, hence, in the limit $P(\omega)\to\infty$, a $P(3\omega)\propto P(\omega)$ dependence is expected.

(iii) Finally, Georges *et al.*[19] pointed out that the ionization of the nonlinear medium may lead to a substantial loss of atoms participating in the process of harmonic generation. Taking into account power broadening, Stark shifts and ionization losses, they claim very good agreement of their theory with the experimental results of Ward and Smith.[4]

All these investigations have been performed without considering phase-matching effects or the depletion of the fundamental wave due to two-photon absorption. For the interpretation of the Ward and Smith experiment, these approximations are valid, since the experiment was performed in a pure Cs-vapor cell with its density N and length L adjusted to approximately one coherence length. Their column density $NL\simeq6\times10^{16}$ cm^{-2} was so small that, even for a complete saturation of the resonant levels, the attenuation of the fundamental wave and the resulting change of the coherence length was negligible. (In normally dispersive systems the coherence length may even increase with increasing population of the upper resonant level.[20]) Such a low-density system, however, has

one severe disadvantage: Since the column density NL is limited by the coherence length, which normally imposes a rather low value on NL, a large harmonic output can only be achieved with large input intensities, and, hence, very soon the saturation limit due to power broadening and the Stark shifts is reached.

In our recent paper[11] on resonant THG in Sr, we have demonstrated that by adding Xe to the system[21] perfect phase matching is possible with NL as large as 2×10^{18} cm^{-2}. Owing to this large number of interacting atoms, much lower input intensities are acceptable, making the influence of Stark shifts and power broadening less pronounced. Nevertheless, the high-density system shows saturation, as it will be shown in Sec. IV, but for different physical reasons. Here, the depletion of the fundamental wave due to two-photon absorption can no longer be neglected, and even small changes of the initial population distribution induced by the two-photon absorption will influence the phase-matching properties of the system.

Since the high-density system appears to us more promising for reasons outlined in the following sections, we present in this paper a theoretical and experimental investigation of its properties. In Sec. II the theory of quasistationary resonant THG is outlined including depletion of the fundamental wave and changes of the phase-matching condition due to changes of the level populations. Analytical expressions for the generated third-harmonic intensity and the optimum experimental parameters such as initial mismatch and atomic column density NL are given. In Sec. III the experimental setup for the investigation of saturation effects is described. The experiments were performed in a Sr-Xe mixture, using a flash-lamp-pumped dye laser tuned to the $5s^2$–$5s5d$ two-photon resonance of Sr. In Sec. IV the experimental results and a comparison with theory are presented.

II. THEORY

In this section an analytical description of resonant THG is given based on the following model: We consider the interaction of two plane electromagnetic waves with a gaseous nonlinear medium, such as a metal vapor, as they propagate along the medium. The two electromagnetic waves, the fundamental and the generated harmonic, are assumed to be monochromatic. The nonlinear medium is approximated by the 4-level system shown in Fig. 1. The frequency of the fundamental wave is tuned to exact resonance with the two-photon transition $|1\rangle \rightarrow |2\rangle$, i.e., $2\omega = (E_2 - E_1)/\hbar = \Omega_{21}$. Level 3 stands for all the intermediate levels

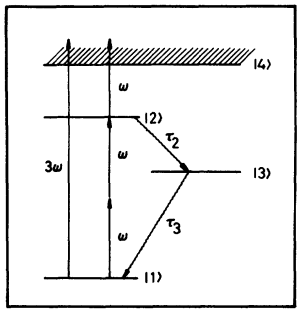

FIG. 1. 4-level system indicating the relevant energy levels for two-photon resonant third-harmonic generation. State $|3\rangle$ stands for the intermediate states, whereas state $|4\rangle$ represents the ionization continuum.

through which the population of the upper resonant level 2 may relax with the lifetimes τ_2 and τ_3, respectively. Level 4 represents the continuum which may be reached from the ground state $|1\rangle$ by the absorption of either one harmonic photon or three fundamental photons.

With the slow-amplitude approximation, the propagation of the electromagnetic waves through the nonlinear medium can be written as

$$\frac{d\hat{E}_q}{dz} = i\,\frac{2\pi(q\omega)^2}{c^2 k_q}\,\vec{P}_q^{\,NL}\exp(-ik_q z) - \tfrac{1}{2}\sigma_1^{(1)}(q\omega)N_1\hat{E}_q\ , \tag{1}$$

where $\vec{E}_q = \hat{E}_q \exp(ik_q z)$ and $\vec{P}_q^{\,NL}$ are the Fourier components of the electric field and of the nonlinear polarization at the frequency $q\omega$. Note that the definition of the wave vector $k_q = q\omega n_q/c$ includes the linear refractive index n_q, whereas all the remaining phases are included in the complex amplitudes $\hat{E}_q$. In the following we set $n_q = 1$, except for the differences of the refractive indices. N_1 is the number density of the ground state of the nonlinear medium and

$$\sigma_1^{(1)}(q\omega) = (4\pi q\omega/c)\tilde{\chi}_1^{(1)}(q\omega) \tag{2}$$

is the one-photon absorption cross section at the frequency $q\omega$, with $\tilde{\chi}_1^{(1)}(q\omega)$ being the imaginary part of the linear susceptibility with respect to the ground state

$$\chi_1^{(1)}(q\omega) = \sum_k \frac{|\mu_{k0}|^2}{\hbar(\omega_{k0} - q\omega)}\ . \tag{3}$$

μ_{k0} is the dipole matrix element for the transition $|0\rangle \rightarrow |k\rangle$ and $\omega_{k0} = \Omega_{k0} - i\Gamma_{k0}$ is the corresponding complex transition frequency with the linewidth Γ_{k0}.

The response of the nonlinear medium to the incident electromagnetic fields is contained in the nonlinear polarization $\vec{P}_q^{\,NL}$. There are two different approaches in evaluating $\vec{P}_q^{\,NL}$.

(a) In the first method the density matrix formalism is used throughout and $\vec{P}_q^{NL}$ is finally derived from the relation $P = \mathrm{Tr}(\rho\mu)$.[20, 22-23] This procedure yields intensity-dependent susceptibilities per atom, since all the intensity-dependent effects associated, for example, with the absorption processes are directly included. The main advantage of this approach is that it includes all the significant effects, such as Stark shifts of the atomic levels, saturation of the resonant transition, and coherent excitations. For a multilevel system, however, the resulting set of equations becomes somewhat complex and the different physical processes taking place in the medium are hard to distinguish.

(b) The other approach treats the atoms which are excited to different energy levels as different atoms with their own constant nonlinear susceptibility, which can be found from ordinary perturbation theory[24-25] taking the corresponding excited states as the initial state: The total nonlinear polarization of the medium is then found from a summation over all the excited states, whose populations are calculated from a rate-equation system.

In our analysis we use the latter approach. We are well aware of the fact that one has to be careful with rate equations at high intensities. However, since we are interested in a steady-state solution, there is no problem. In this case the advantage of the rate-equation system is that the physical processes become more transparent. Furthermore, approximations and their limits of validity are more easily discussed.

In this case we can write the nonlinear polarization as

$$\vec{P}_1^{NL} = \sum_i \{ \tfrac{1}{4} N_i [3\chi_{iT}^{(3)}(3\omega)\vec{E}_3\vec{E}_1^*\vec{E}_1^* + \chi_{iS}^{(3)}(\omega)\vec{E}_1|\vec{E}_1|^2 + \chi_{iS}^{(3)}(\omega, 3\omega)\vec{E}_1|\vec{E}_3|^2] - (N_{0i} - N_i)\chi_i^{(1)}(\omega)\vec{E}_1 \},$$

$$\vec{P}_3^{NL} = \sum_i \{ \tfrac{1}{4} N_i [\chi_{iT}^{(3)}(3\omega)\vec{E}_1\vec{E}_1\vec{E}_1 + \chi_{iS}^{(3)}(3\omega)\vec{E}_3|\vec{E}_3|^2 + \chi_{iS}^{(3)}(3\omega, \omega)\vec{E}_3|\vec{E}_1|^2] - (N_{0i} - N_i)\chi_i^{(1)}(3\omega)\vec{E}_3 \}. \quad (4)$$

The first three terms in Eq. (4) represent the contribution of level i to the three independent third-order nonlinear susceptibilities, whereas the last term describes the changes of the refractive index of the system due to the absorption-induced population changes. $\chi_i^{(1)}$ is the linear susceptibility of level i, whose initial number density is N_{0i}. Usually $N_{0i} = N_0$ for $i = 1$ and $N_{0i} = 0$ for $i \neq 1$ holds, where N_0 is the total number density of the nonlinear system.

For resonant THG the third-order nonlinear susceptibilities evaluated from perturbation theory[25] may be separated into a resonant part $\chi_R^{(3)}$ containing the resonant transition $|1\rangle \rightarrow |2\rangle$, and a nonresonant part $\chi_{NR}^{(3)}$ covering the contributions of all the other transitions. For our purpose we restrict ourselves to the resonant parts, which are orders-of-magnitude larger than the nonresonant parts for systems operating near resonance. Hence, we may write the nonlinear susceptibility responsible for THG,

$$\chi_T^{(3)}(3\omega) \simeq \chi_{TR}^{(3)}(3\omega) = \frac{1}{\hbar(\omega_{21} - 2\omega)} \left(\sum_k \frac{\mu_{1k}\mu_{k2}}{\hbar(\omega_{k1} - \omega)} \right) \times \left(\sum_k \frac{\mu_{1k}\mu_{k2}}{\hbar(\omega_{k1} - 3\omega)} \right). \quad (5)$$

ω_{21} stands for the complex transition frequency of the resonant transition $|1\rangle \rightarrow |2\rangle$. In general, $\omega_{21} = \Omega_{21} + \delta\Omega_{21} - i\Gamma_{21}$ includes the unperturbed energy separation of both levels, $\Omega_{21} = (E_2 - E_1)/\hbar$, the relative Stark shift of the levels, $\delta\Omega_{21} = (1/4\hbar)[\chi_2^{(1)}(\omega) - \chi_1^{(1)}(\omega)]|\hat{E}_1|^2$, and the linewidth of the transition Γ_{21}. In our analysis, however, we neglect the Stark shift, since for the intensity range discussed below it is much smaller than the laser linewidth used in the experiment. Furthermore, we adopt the concept of the experimentally determined effective linewidth Γ_{eff} introduced in our recent paper,[11] which is valid as long as the Doppler width is small compared to the laser linewidth. Hence, we replace in Eq. (5) $\omega_{21} - 2\omega$ by $(\Omega_{21} - 2\omega) - i\Gamma_{eff}$. It should be noted that power-broadening is not contained in Γ_{eff}, but results from the rate equations.

Expressions similar to Eq. (5) can be derived for the resonant parts of the other two third-order nonlinear susceptibilities, namely,

$$\chi_S^{(3)}(\omega) \simeq \chi_{SR}^{(3)}(\omega) = \frac{2}{\hbar(\omega_{21} - 2\omega)} \left(\sum_k \frac{\mu_{1k}\mu_{k2}}{\hbar(\omega_{k1} - \omega)} \right)^2 \quad (6)$$

and

$$\chi_S^{(3)}(3\omega, \omega) \simeq \chi_{SR}^{(3)}(3\omega, \omega) = \frac{1}{\hbar(\omega_{21} - 2\omega)} \left(\sum_k \frac{\mu_{1k}\mu_{k2}}{\hbar(\omega_{k1} - 3\omega)} \right)^2. \quad (7)$$

In the following we use the notation $\chi_S^{(3)} = \bar{\chi}_S^{(3)} + i\tilde{\chi}_S^{(3)}$, where the real parts $[\bar{\chi}_S^{(3)}(\omega)$ and $\bar{\chi}_S^{(3)}(3\omega, \omega)]$ are responsible for the intensity-depend-

ent refractive indices (Kerr effect), and the imaginary parts describe the two-photon absorption $[\tilde{\chi}_S^{(3)}(\omega)]$ and the Raman scattering $[\tilde{\chi}_S^{(3)}(3\omega,\omega) = \tilde{\chi}_S^{(3)}(\omega,3\omega)]$, respectively. In this notation the two-photon absorption cross section is given by

$$\sigma^{(2)}(\omega) = (\pi\omega/c)\tilde{\chi}_S^{(3)}(\omega)|\hat{E}_1|^2 = 2\omega(2\pi/c)^2\tilde{\chi}_S^{(3)}(\omega)\Phi_1 , \quad (8)$$

where $\Phi_1 = (8\pi/c)|\hat{E}_1|^2$ is the intensity of the fundamental wave. In the steady-state limit, the populations of the different levels shown in Fig. 1 can be readily written down as

$$N_1 = N_0[1 + (g_1/g_2)\tau_2\sigma^{(2)}(\omega)\Phi_1/2\hbar\omega]/[1 + (\Phi_1/\Phi_S)^2],$$
$$N_2 = N_0[\tau_2\sigma^{(2)}(\omega)\Phi_1/2\hbar\omega]/[1 + (\Phi_1/\Phi_S)^2], \quad (9)$$
$$N_3 = N_2\tau_3/\tau_2 ,$$

and

$$\Delta N = N_1 - N_2(g_1/g_2) = N_0/(1 + \Phi_1^2/\Phi_S^2) \quad (10)$$

being the population difference of the resonant levels, where

$$\Phi_S = (c/2\pi)\{[\tau_3 + \tau_2(1 + g_1/g_2)]\tilde{\chi}_S^{(3)}(\omega)/\hbar\}^{-1/2} \quad (11)$$

is the saturation intensity. Here we took into account the degeneracy of the resonant levels by their statistical weights g_1 and g_2, respectively. The population of the continuum is neglected in this model, since for a significant direct one-photon ionization from the ground state, the harmonic intensities under consideration are by far too low. In contrast to the Cs experiment by Ward and Smith, for our experiments described in the following sections, the three-photon ionization via the resonant two-photon transition is also negligible, since the absorption cross section for the $|2\rangle \rightarrow |4\rangle$ transition in Sr at a wavelength of 575.7 nm is calculated[26] to be 3×10^{-21} cm^2. Hence, the population N_4 of the continuum would amount to only 1% of the population of the upper resonant level at an input energy of 1 J/cm^2.

From Eq. (9) the population density N_i of level i can be evaluated and expressed in terms of the population difference ΔN and the fundamental intensity Φ_1. For the last term in Eq. (4) one then can write

$$-\sum_i (N_{0i} - N_i)\chi_i^{(1)}(q\omega) = \Delta N\,\frac{\sigma^{(2)}(\omega)}{2\hbar\omega}\,\Phi_1[\tau_i\chi_{i1}^{(1)}(q\omega)], \quad (12)$$

where

$$[\tau_i\chi_{i1}^{(1)}(q\omega)] \equiv \sum_i \tau_i[\chi_i^{(1)}(q\omega) - \chi_1^{(1)}(q\omega)] \quad (13)$$

uses Einstein's sum convention. $\chi_i^{(1)}(q\omega)$ stands for the linear susceptibility of level i, averaged over all its sublevels.

Inserting now Eqs. (4) and (12) into Eq. (1) and neglecting all terms proportional to the third-harmonic intensity, which is assumed to be much lower than the fundamental intensity, we finally get for the Fourier components of the electric field at ω and 3ω the following two equations:

$$\frac{d\hat{E}_1}{dz} = i\frac{\pi\omega}{2c}\Delta N\left(\chi_S^{(3)}(\omega)|\hat{E}_1|^2\hat{E}_1 + \frac{[\tau_i\chi_{i1}^{(1)}(\omega)]}{4\hbar}\tilde{\chi}_S^{(3)}(\omega)|\hat{E}_1|^4\hat{E}_1\right), \quad (14a)$$

$$\frac{d\hat{E}_3}{dz} = i\frac{\pi 3\omega}{2c}\Delta N\left(\chi_T^{(3)}(3\omega)\hat{E}_1^3\exp(i\Delta kz) + \chi_S^{(3)}(3\omega,\omega)|\hat{E}_1|^2\hat{E}_3 + \frac{[\tau_i\chi_{i1}^{(1)}(3\omega)]}{4\hbar}\tilde{\chi}_S^{(3)}(\omega)|\hat{E}_1|^4\hat{E}_3\right)$$
$$-\sigma^{(1)}(3\omega)\frac{\Delta N}{2}\hat{E}_3\left(1 + \frac{g_1}{g_2}\frac{\tau_2\tilde{\chi}_S^{(3)}(\omega)}{16\hbar}|\hat{E}_1|^4\right), \quad (14b)$$

with $\Delta k = 3k_1 - k_3$ being the initial wave-vector mismatch of the fundamental and the harmonic wave.

Before going on in solving Eq. (14), let us summarize the most important assumptions which led to the above equations.

(1) The Stark shift of the atomic levels is neglected, since the laser linewidth is assumed to be much larger.

(2) The population changes due to two-photon absorption are evaluated from a stationary rate equation system. Their influence on the nonlinear susceptibilities, i.e., power broadening and their action on the phases of the electric fields [second term in Eq. (14)] are taken into account.

(3) The attenuation of the generated harmonic wave due to one-photon absorption is taken into account [third term in Eq. (14b)], including the intensity-dependent ground-state population. The corresponding population of the continuum, however, is neglected.

(4) Depletion of the fundamental wave takes place only due to the resonant two-photon absorption [first term in Eq. (14a)].

All these assumptions can be met in the experiment by proper adjustment of the experimental

parameters. It is a model, which in nearly all respects contrasts existing models. One may call it a high-density model, since the two important aspects, namely the attenuation of the fundamental wave due to the two-photon absorption and the resulting changes in phase matching, are closely related to a relatively large number density of the nonlinear medium. It will be shown below, however, that in resonant THG it is more advantageous to work in the high-density than in the low-density regime, where the resonant transition easily saturates.

A. Analytical solutions

We now proceed with the discussion of Eq. (14). With $\hat{E}_1 = \rho_1 \exp(i\varphi_1)$, Eq. (14a) can be rewritten as

$$\frac{d\rho_1}{dz} = -\frac{\pi\omega}{2c}\tilde{\chi}_S^{(3)}(\omega)\Delta N\rho_1^3 = -\frac{\pi\omega}{2c}\tilde{\chi}_S^{(3)}(\omega)N_0\rho_1^3/(1+\rho_1^4/\rho_S^4) \tag{15a}$$

$$\frac{d\varphi_1}{dz} = \frac{\pi\omega}{2c}\bar{\chi}_S^{(3)}(\omega)\Delta N\rho_1^2 + \frac{\pi\omega}{8\hbar c}\Delta N\tilde{\chi}_S^{(3)}(\omega)[\tau_i\chi_{i1}^{(1)}(\omega)]\rho_1^4 \tag{15b}$$

with $\rho_S^2 = (8\pi/c)\Phi_S$. Integrating Eq. (15a) from $z=0$ to $z=L$, we get an implicit expression for $\Phi_1(L)$, namely,

$$(\Phi_0 - \Phi_1)(\Phi_S^2 + \Phi_0\Phi_1)/(\Phi_1\Phi_S^2) = \alpha_2 L\ , \tag{16}$$

with $\alpha_2 = N_0\,\sigma_0^{(2)}(\omega)$ being the two-photon absorption coefficient at the input intensity $\Phi_0 = \Phi_1$ $(z=0)$.

Because of the complex dependence of the fundamental intensity Φ_1 on the length z, it is more convenient to choose ρ_1 as the new variable instead of z. Dividing Eq. (14b) by Eq. (15a) and writing $\hat{E}_3 = E_3\exp[i(\Delta kz + 3\varphi_1)]$, we can integrate the resulting equation from $\rho_1 = \rho_0$ up to $\rho_1 = \rho_L$ and finally get

$$E_3 = -3i[\chi_T^{(3)}(3\omega)/\tilde{\chi}_S^{(3)}(\omega)]\exp\left(\int_{\rho_0}^{\rho_L} F(\rho_1)d\rho_1\right)\int_{\rho_0}^{\rho_L}\exp\left(-\int_{\rho_0}^{\rho_1'} F(\rho_1)d\rho_1\right)d\rho_1' \tag{17}$$

with

$$F(\rho_1) = \frac{2}{\alpha_2\rho_0}\left[\beta\frac{\rho_1}{\rho_0} - \gamma\left(\frac{\rho_0}{\rho_1}\right)^3 + \delta\frac{\rho_0}{\rho_1}\right]. \tag{18}$$

Here we introduced the following abbreviations:

$$\beta = \bar{\beta} + i\tilde{\beta} = \frac{\sigma^{(1)}(3\omega)(g_1/g_2)\tau_2\alpha_2}{4\hbar\omega}\Phi_0 + i\left[\Delta k\left(\frac{\Phi_0}{\Phi_S}\right)^2 + (\tau_i\Delta\chi_i^{(1)})\frac{3\pi\alpha_2}{c\hbar}\Phi_0\right], \tag{19a}$$

$$(\tau_i\Delta\chi_i^{(1)}) = [\tau_i\chi_{i1}^{(1)}(\omega)] - [\tau_i\chi_{i1}^{(1)}(3\omega)], \tag{19b}$$

$$\gamma = \bar{\gamma} + i\tilde{\gamma} = -\tfrac{1}{2}\sigma^{(1)}(3\omega)N_0 - i\Delta k\ , \tag{19c}$$

$$\delta = \bar{\delta} + i\tilde{\delta} = 3\omega(2\pi/c)^2[\chi_S^{(3)}(3\omega,\omega) - \tilde{\chi}_S^{(3)}(\omega)]N_0\Phi_0\ . \tag{19d}$$

Their physical significance is as follows: γ stands for the one-photon absorption coefficient (real part, $\bar{\gamma}$) and the initial mismatch of the system (imaginary part, $\tilde{\gamma}$). $\bar{\beta}$, the real part of β, takes into account the changes of the one-photon absorption coefficient due to the depletion of the ground state, whereas the imaginary part $\tilde{\beta}$ is the mismatch associated with the population changes of the nonlinear medium. Finally, δ represents the intensity-dependent mismatch due to the Kerr effect (real part, $\bar{\delta}$) and the Raman scattering coefficient (imaginary part, $\tilde{\delta}$).

In the following we restrict our discussion to exact resonance, where the real part of δ vanishes. We neglect also its imaginary part, since one can show that because of the large denominator of the Raman susceptibility [see Eq. (7)] for most of the nonlinear materials, $\chi_S^{(3)}(3\omega,\omega)$ is at least two orders of magnitude smaller than $\chi_S^{(3)}(\omega)$.

The integral $\int_{\rho_0}^{\rho_L} F(\rho_1)d\rho_1$ in Eq. (17) can be readily performed, yielding

$$\int_{\rho}^{\rho_L} F(\rho_1)d\rho = \frac{1}{\alpha_2}\left[\beta\left(\frac{\rho_L}{\rho_0}\right)^2 + \gamma\left(\frac{\rho_0}{\rho_L}\right)^2 - \beta - \gamma\right] = -\frac{1}{\alpha_2}\left[\beta - \gamma\left(\frac{\rho_0}{\rho_L}\right)^2\right]\left[1 - \left(\frac{\rho_L}{\rho_0}\right)^2\right]. \tag{20}$$

The imaginary part of this equation is a measure for the total change of the mismatch due to dispersion along the length L.

Expressing now the amplitude of the fundamental wave at a distance z in terms of the transmission of the system

$$T = \Phi_1(z)/\Phi_1(z=0) = (\rho_1/\rho_0)^2\ , \tag{21}$$

the remaining integral in Eq. (17) can be cast into the form $\int\exp(-a^2T - b^2/T)d\sqrt{T}$, whose solution may be given in terms of complex error functions.[27] After some tedious algebra, we get for the intensity of the generated third-harmonic

$$\Phi_3 = \left|\frac{3\chi_T^{(3)}(3\omega)}{\tilde{\chi}_S^{(3)}(\omega)}\right|^2 \Phi_0 \left|\frac{\pi\alpha_2}{16\beta}\right| \left| \exp(y_+^2)[\mathrm{erf}(y_+) - \mathrm{erf}(y_{1+})] + \exp(y_-^2)[\mathrm{erf}(y_-) - \mathrm{erf}(y_{1-})] \right|^2, \tag{22}$$

with $y_\pm = \sqrt{\beta T/\alpha_2} \pm \sqrt{\gamma/T\alpha_2}$ and $y_{1\pm} = \sqrt{\beta/\alpha_2} \pm \sqrt{\gamma/\alpha_2}$. A general discussion of this solution is rather cumbersome. If, however, one is interested in the evaluation of the optimum conditions and an insight of how the different material parameters act on the system, Eq. (22) is very useful.

Let us first consider the case $\beta = 0$; i.e., we neglect the influence of changes in the level populations. Either from Eq. (22) taking the limit $\beta \to 0$ or from direct integration of Eq. (17), which is more convenient, we get for the intensity conversion

$$\eta \equiv \frac{\Phi_3}{\Phi_0} \simeq \left|\frac{3\chi_T^{(3)}(3\omega)}{\tilde{\chi}_S^{(3)}(\omega)}\right|^2 \exp\left[-\frac{\alpha_1}{\alpha_2}\left(\frac{1}{T}-1\right)\right] \left| 1 - \sqrt{T}\exp\left[-\frac{\gamma}{\alpha_2}\left(\frac{1}{T}-1\right)\right] - \left(\frac{\pi\gamma}{\alpha_2}\right)^{1/2} \exp\left(\frac{\gamma}{\alpha_2}\right)\left[\mathrm{erf}\left(\frac{\gamma}{T\alpha_2}\right)^{1/2} - \mathrm{erf}\left(\frac{\gamma}{\alpha_2}\right)^{1/2}\right] \right|^2. \tag{23}$$

Depending on the ratio of the one-photon to two-photon absorption coefficient, α_1/α_2, we may rewrite Eq. (23) in the two forms

$$\eta \simeq \left|\frac{12\pi^2\omega}{c^2\gamma} N_0 \chi_T^{(3)}(3\omega)\Phi_0\right|^2 \left\{1 + T^3 \exp\left[-\frac{\alpha_1}{\alpha_2}\left(\frac{1}{T}-1\right)\right] - 2T^{3/2}\cos\left[\frac{\Delta k}{\alpha_2}\left(\frac{1}{T}-1\right)\right]\exp\left[-\frac{\alpha_1}{2\alpha_2}\left(\frac{1}{T}-1\right)\right]\right\} \tag{24a}$$

for $\alpha_1/2 \leq |\gamma| \gg \alpha_2$, and

$$\eta \simeq \left|\frac{3\chi_T^{(3)}(3\omega)}{\tilde{\chi}_S^{(3)}(\omega)}\right|^2 \left\{T + \exp\left[-\frac{\alpha_1}{\alpha_2}\left(\frac{1}{T}-1\right)\right] - 2\sqrt{T}\cos\left[\frac{\Delta k}{\alpha_2}\left(\frac{1}{T}-1\right)\right]\exp\left[-\frac{\alpha_1}{2\alpha_2}\left(\frac{1}{T}-1\right)\right]\right\} \tag{24b}$$

for $\alpha_1/2 \leq |\gamma| \ll \alpha_2$.

The preceding equations look quite similar. In both cases optimum results are achieved for zero initial mismatch $\Delta k = 0$. At low input intensities the conversion increases with the square of the input intensity [Eq. (24a)] and the optimum values for density and length are reached when the medium is optically thick with respect to the one-photon absorption.[11] Note that in this case the transmission T can be approximated by $T \simeq (1+\alpha_2 L)^{-1}$ and $-(\alpha_1/\alpha_2)[(1/T)-1]$ becomes $(-\alpha_1 L)$. Raising the input intensity up to a level where the two-photon absorption coefficient overtakes the one-photon absorption coefficient [Eq. (24b)], the conversion reaches asymptotically with $\alpha_1 \to 0$ a maximum value of

$$\eta_{\max} = |3\chi_T^{(3)}(3\omega)/\tilde{\chi}_S^{(3)}(\omega)|^2, \quad \text{for } \beta = 0 \tag{25}$$

as the medium becomes optically thick, now with respect to the two-photon absorption. Similar to nonresonant THG,[14] the maximum conversion efficiency depends only on the nonlinear susceptibilities of the medium.

This result, which was already obtained by other authors,[23,28] gives an upper limit for the harmonic conversion under ideal conditions, namely for perfect phase matching throughout the interaction region of the light waves. For realistic systems this assumption is only valid at low input intensities, where the population changes induced by the two-photon absorption can be neglected even with respect to the phases.

To include the latter effect we have to return to Eq. (22) allowing for $\beta \neq 0$. From a numerical analysis of Eq. (22) we found that optimum conditions for THG with respect to the mismatch Δk are achieved if the relation

$$\tilde{\beta} - \tilde{\gamma}(\rho_0/\rho_L)^2 \equiv \tilde{\beta} - \tilde{\gamma}/T = 0 \tag{26}$$

is satisfied, giving rise to an optimum mismatch

$$\Delta k_{\mathrm{opt}} = -(\tau_i \Delta\chi_i^{(1)})\left(\frac{3\pi\alpha_2}{c\hbar}\right) T\Phi_0 \frac{\Phi_S^2}{\Phi_S^2 + \Phi_0^2 T}. \tag{27}$$

The physical interpretation of this relation becomes quite obvious comparing Eq. (26) with Eq. (20). It shows that the generated third-harmonic intensity approaches a maximum, if the total mismatch, integrated along the distance under consideration, vanishes. Nevertheless, this numerical finding was somewhat surprising, since we were not able to prove Eq. (26) analytically for arbitrary experimental conditions. We succeeded only in showing that for $\alpha_1 = 0$ and low input inten-

sities ($\Phi_0 \ll \Phi_S$), Eq. (26) can be deduced analytically.[29] Our numerical calculations, presented in the Sec. II B, revealed, however, that Eq. (26) retains its validity even for $\alpha_1 \neq 0$ and $\Phi_0 \geq \Phi_S$ and reproduces the numerical values for the optimum mismatch with an error of less than 1%.

In the following we will neglect the one-photon absorption ($\alpha_1 = 0$) leaving this complication for the numerical discussion presented in the Sec. II B. With the optimum conditions for Δk, the third-harmonic intensity can be calculated inserting Eq. (26) into Eq. (22). After some tedious algebra one obtains

$$\Phi_3 = \left| \frac{3\chi_T^{(3)}(3\omega)}{\tilde{\chi}_S^{(3)}(\omega)} \right|^2 \frac{c\hbar}{6|\tau_i \Delta\chi_i^{(1)}|} \times \left(1 + \frac{T\Phi_0^2}{\Phi_S^2}\right)[C^2(x) + S^2(x)], \quad (28)$$

where $C(x) = \int_0^x \cos(\frac{1}{2}\pi u^2)\, du$ and $S(x) = \int_0^x \sin(\frac{1}{2}\pi u^2)\, du$ are the Fresnel integrals with the argument

$$x = (1 - \sqrt{T}) \left(\frac{6|\tau_i \Delta\chi_i^{(1)}| \Phi_0 \Phi_S^2}{c\hbar (\Phi_S^2 + T\Phi_0^2)} \right)^{1/2}.$$

Equation (28) has some interesting properties which follow.

(a) For $\Phi_0 \ll \Phi_S$, we may write $(1 + T\Phi_0^2/\Phi_S^2) \simeq 1$ and the third-harmonic intensity is proportional only to $[C^2(x) + S^2(x)]$, which has an absolute maximum of 0.9, reached for an argument $x = 1.21$ (Ref. 27). Hence, in this case, we get a constant maximum harmonic intensity

$$\Phi_{3\max} = \frac{0.9\hbar c}{6|\tau_i \Delta\chi_i^{(1)}|} |3\chi_T^{(3)}(3\omega)/\tilde{\chi}_S^{(3)}(\omega)|^2, \quad \Phi_0 \ll \Phi_S \quad (29)$$

which depends only on the material parameters of the nonlinear medium. The optimum experimental conditions for reaching this value are expressed in terms of the phase-matching condition of Eq. (27) and, with respect to the length, number density and input intensity are given by $T \simeq (1 + \alpha_2 L)^{-1}$ and the relation $x = 1.21$. This leads to

$$(N_0 L)_{\text{opt}} \simeq \left(\frac{8\pi}{c}\Phi_0\right)^{-3/2} \left(\frac{4c\hbar\, 1.21}{3\pi\omega\tilde{\chi}_S^{(3)}(\omega)|\tau_i \Delta\chi_i^{(1)}|} \right), \quad \text{for } \Phi_0 \ll \Phi_S \quad (30)$$

as long as $6|\tau_i \Delta\chi_i^{(1)}|\Phi_0/c\hbar \gg 1.5$. For $6|\tau_i \Delta\chi_i^{(1)}|\Phi_0/c\hbar \leq 1.5$, the optimum length as well as the optimum input intensity approaches infinity, indicating that in this regime the influence of the intensity-dependent mismatch is negligible, and Eqs. (23–25) are applicable.

From Eq. (30) it follows that by increasing the input intensity Φ_0, the product $N_0 L$ can always be made small enough to fulfill the condition $\alpha_1 L \ll 1$, which justifies our assumption $\alpha_1 = 0$ used in the derivation of the above equations, as long as the input intensity Φ_0 stays below the saturation intensity Φ_S.

(b) for $\Phi_0 \gg \Phi_S$ we have to consider in Eq. (28) the factor $[1 + T(\Phi_0/\Phi_S)^2]$. Evaluating the derivative of Φ_3 with respect to T, one can show that the maximum conversion efficiency becomes a constant, namely,

$$\eta_{\max} = \left| \frac{3\chi_T^{(3)}(3\omega)}{\tilde{\chi}_S^{(3)}(\omega)} \right|^2, \quad \beta \neq 0, \quad \Phi_0 \gg \Phi_S. \quad (31)$$

The corresponding optimum experimental conditions are again expressed in terms of the phase-matching condition of Eq. (27) and, with respect to the length, number density and input intensity are given by the relations $(1 - T) \simeq \alpha_2 L(\Phi_S/\Phi_0)^2$ and $T \ll 1$. This yields

$$(N_0 L)_{\text{opt}} \simeq \left(\frac{c}{2\pi}\right)^2 \frac{\Phi_0}{2\omega\tilde{\chi}_S^{(3)}(\omega)\Phi_S^2}, \quad \Phi_0 \gg \Phi_S. \quad (32)$$

The preceding results indicate that there are only small population changes as long as the input intensity is well below the saturation intensity. However, the resulting phase shift imposes a severe limitation to the maximum attainable harmonic intensity. This is due to the intensity-dependent phase shift, which cannot be compensated by the initial mismatch throughout the medium as the fundamental intensity drops from Φ_0 to $T\Phi_0$.

For input intensities well above the saturation intensity there is, on the other hand, a large change of the population densities, and the phase shift due to the different refractive indices of the populated levels is also significant. This phase shift, however, can be compensated by a proper initial mismatch, even over large distances. The medium is almost equally populated in the upper and lower levels, $|1\rangle$ and $|2\rangle$, and a depletion of the fundamental intensity does not alter this population significantly as long as the intensity remains well above the saturation intensity.

B. Numerical solution

The analytical solutions derived in Sec. II A were useful for determining power laws and upper limits for the harmonic intensity. This, however, was only possible for one of the experimental or material parameters being dominant. In order to find how the asymptotic values are reached and how the system acts if all the different physical processes are of similar importance, one has to evaluate Eq. (14) numerically.

First, we use the numerical solutions to show how sensitive the harmonic output is to changes of the experimental parameters (length and initial mismatch). The calculations are performed with

the nonlinear susceptibilities of Sr when tuning to the $5s^2$-$5s5d$ two-photon resonance: $\lambda = 575.912$ nm, $\chi_T^{(3)}(3\omega) = 1.25\times10^{-30}$ esu, $\tilde{\chi}_S^{(3)}(\omega) = 2.7\times10^{-29}$ esu, $(\tau_i \Delta\chi_i^{(1)}) = -10^{-30}$ esu, and $\sigma^{(1)}(3\omega) = 3.3\times10^{-18}$ cm^2 for an initial particle density $N_0 = 7.2\times10^{16}$ cm^{-3} (8.5 Torr Sr).

In Fig. 2 numerical results for the harmonic intensity versus length are shown for $\Delta k = 0$ and with the fundamental input intensity as a parameter. For comparison, the harmonic output for negligible two-photon absorption (dotted curves) is also given, where the harmonic and the fundamental wave are always in phase ($\Delta k = 0$), but where the harmonic intensity nevertheless tends towards a constant value due to the one-photon absorption. Figure 2 illustrates clearly how in the case of a significant two-photon absorption, both waves come out of phase with increasing input intensity at shorter and shorter distances. This has to be attributed to the change of the refractive indices originating from the population changes induced by the two-photon absorption. For an input intensity of 2×10^7 W/cm^2 the effective coherence length is reduced to less than 1 cm and the resulting harmonic output stays well below the maximum value attainable without two-photon absorption. With increasing length the typical phase-matching oscillations are damped out because the fundamental and the harmonic wave come in phase again as the fundamental wave is attenuated and the intensity-dependent mismatch becomes negligible.

From our analytical solution we learned that this intensity-dependent mismatch can be compensated to some extent by choosing the initial mismatch according to Eq. (27). This is illustrated by Fig. 3 where the harmonic intensity versus length is given for an input intensity of 2×10^7 W/cm^2 with Δk as a parameter. The curve for $\Delta k = 0$ is identical with the solid curve in Fig. 2. Increasing the initial mismatch, one observes an increase in length over which both waves are in phase and the harmonic intensity increases. The optimum output is achieved for a mismatch of $\Delta k = 2.5$ (thick solid curve), where both waves stay in phase over the largest distance. For $\Delta k = 0$, both waves come out of phase before the fundamental experiences a significant attenuation which would lower the total mismatch. For $\Delta k = 3.5$, the mismatch is perfect at the beginning but, as the fundamental is attenuated, the total mismatch is rapidly decreasing and the waves come out of phase. Hence, optimum mismatch results from a compromise: The initial mismatch should be large enough to compensate the intensity-dependent mismatch at the highest input intensity but also sufficiently low to keep the waves in phase over a long enough distance as the intensity-dependent mismatch decreases due to the attenuated fundamental wave. An experimental realization of this compromise increases the harmonic output considerably. In our example this increase amounts to a factor of ~100 for an input intensity of 2×10^7 W/cm^2, compared to phase matching with $\Delta k = 0$.

In order to show how the fundamental wave acts on the nonlinear medium, we have plotted in Fig. 4 the harmonic intensity, the attenuation of the fundamental wave, and the population difference ΔN as a function of length. At the high input intensity of $\Phi_0 = 6.4\times10^8$ W/cm^2, which is well above the saturation intensity (2.7×10^7 W/cm^2), the nonlinear medium is nearly bleached. The population difference ΔN which drives the THG is very small, but, nevertheless, an appreciable increase in third-harmonic intensity can be observed. This is due to the proper adjustment of the initial mismatch $\Delta k = 9.72$ cm^{-1}, which compensates the in-

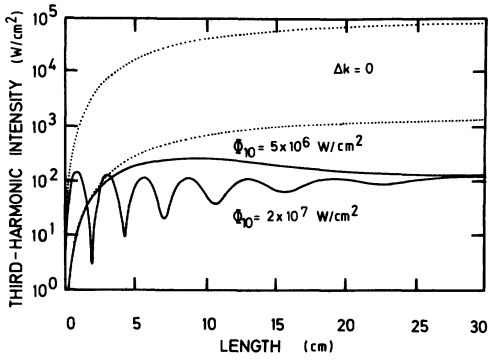

FIG. 2. Third-harmonic intensity versus length of the nonlinear medium for different input intensities of the fundamental wave Φ_{10} and a constant mismatch $\Delta k = 0$. The dotted lines show results with no two-photon absorption (rectangular density distribution).

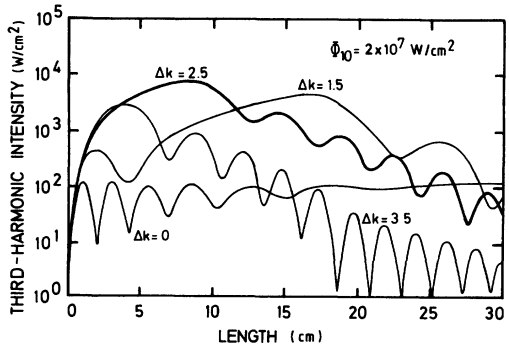

FIG. 3. Third-harmonic intensity versus length of the nonlinear medium for different values of the mismatch Δk and a constant input intensity Φ_{10} (rectangular density distribution).

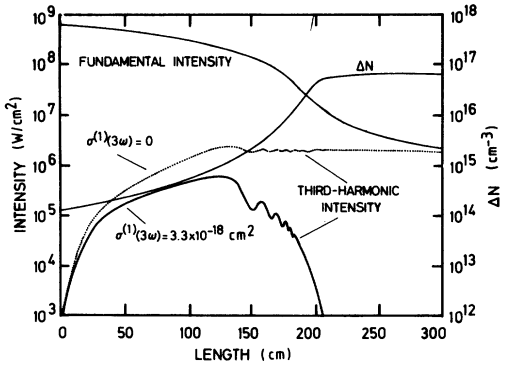

FIG. 4. Third-harmonic intensity, fundamental intensity, and population difference ΔN versus length of the nonlinear medium for an input intensity $\Phi_{10}=6.4\times10^{8}$ W/cm^2. The dotted line shows the third-harmonic intensity for the case of no one-photon absorption.

tensity-dependent mismatch resulting from the small ΔN. The maximum third-harmonic intensity is reached at a length of ~150 cm, up to which the population difference ΔN as well as the fundamental intensity did not change very much. At longer distances ΔN increases very rapidly up to $N_0=7.2\times10^{16}$ cm^{-3} as the fundamental intensity is attenuated down to the saturation intensity. In this region the third-harmonic intensity stays constant (dotted curve) if there is no one-photon absorption, since the driving fundamental intensity became too low for a considerable change of the harmonic intensity. For an existing one-photon absorption (solid curve), however, the harmonic wave is rapidly absorbed by the nonlinear medium. Note that even during the growth of the harmonic wave, the one-photon absorption reduces the harmonic intensity considerably. This is due to the fact that for the one-photon absorption, the ground-state-level population is responsible, whereas for the two-photon absorption the population difference ΔN is responsible. Hence, even at very high input intensities, where the nonlinear medium is bleached, the one-photon absorption coefficient remains a limiting material parameter for THG. At this point we want to give the numerical proof of Eq. (27) for the optimum mismatch. In Table I, the optimum mismatch according to Eq. (27) is given together with the calculated values as a function of the input intensity for three different values of the one-photon absorption coefficient. The values for number density and nonlinear susceptibilities are those specified for Sr at the beginning of this section. Note that the values for Δk found from Eq. (27) agree within less than 1% with the numerical values of all input intensities and absorption cross sections.

One may be surprised at the fact that, for different values of $\sigma^{(1)}(3\omega)$, the numerical as well as the analytical values for Δk are different, although Eq. (27) does not contain $\sigma^{(1)}(3\omega)$ explicitly. This is due to the fact that the optimum length is influenced by $\sigma^{(1)}(3\omega)$, and, hence, the transmission T is changed.

For a given input intensity, the problem of finding the optimum mismatch is therefore shifted to the problem of determining the optimum length. Once this length is found, the optimum mismatch can be given by Eq. (27) with high accuracy. Nevertheless, Eq. (27) is very useful, since one usually wants to know the optimum mismatch for a given experimental setup. Since the length is given and the transmission T is known, one can readily determine the optimum mismatch from Eq. (27).

We now proceed to check the upper limits for the harmonic generation. For this purpose, we have solved Eq. (14) numerically including the population saturation. The results are shown in Fig. 5, where the optimum harmonic intensity is

TABLE I. Optimum mismatch Δk as a function of the input intensity Φ_0 for three different values of the one-photon absorption cross section $\sigma^{(1)}(3\omega)$. Δk_{num} is obtained from a numerical integration. Δk_{an} is given by Eq. (27). Δk has been calculated for $(\tau_i\Delta\chi_i^{(1)})=-9.9\times10^{-31}$ esu, $\chi_T^{(3)}=1.25\times10^{-30}$ esu, $\chi_S^{(3)}=2.13\times10^{-29}$ esu, and $N_0=7.2\times10^{16}$ cm^{-3}.

	$\sigma^{(1)}(3\omega)=0$		$\sigma^{(1)}(3\omega)=3.3\times10^{-18}$ cm^2		$\sigma^{(1)}(3\omega)=3.3\times10^{-17}$ cm^2	
Φ_0	Δk_{num}	Δk_{an}	Δk_{num}	Δk_{an}	Δk_{num}	Δk_{an}
2.5×10^6	0.016 12	0.016 03	0.064 03	0.065 96	0.068 97	0.077 49
5×10^6	0.118 12	0.117 47	0.224 73	0.234 08	0.289 96	0.294 95
1×10^7	0.625 31	0.620 52	0.770 80	0.794 94	1.020 66	1.041 5
2×10^7	2.404 9	2.382 8	2.489 4	2.521 6	2.916 0	3.021 3
4×10^7	5.649 1	5.604 2	5.713 3	5.697 6	6.034 6	6.106 0
8×10^7	8.191 3	8.154 6	8.211 4	8.196 2	8.352 7	8.402 2
1.6×10^8	9.260 9	9.242 5	9.268 5	9.263 5	9.321 83	9.353 0
3.2×10^8	9.614 4	9.605 2	9.619 3	9.617 4	9.569 6	9.625 1
6.4×10^8	9.723 1	9.718 0	9.721 5	9.723 6	9.706 8	9.722 6
1.28×10^9	9.756 6	9.753 9	9.750 5	9.755 2	9.749 9	9.751 0

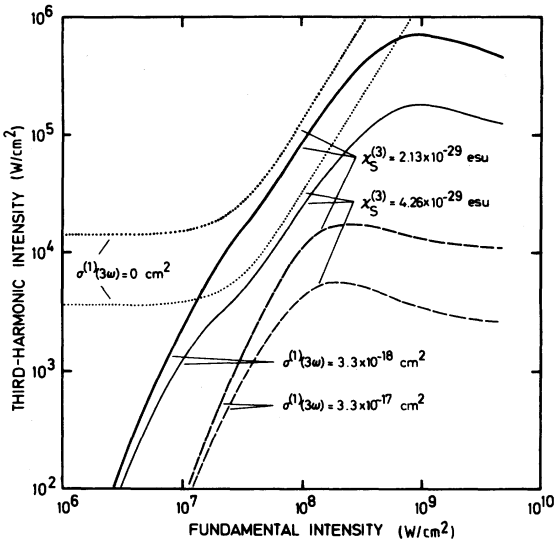

FIG. 5. Third-harmonic intensity versus fundamental intensity for different values of the one-photon and two-photon absorption cross sections.

plotted as a function of the input intensity for three different one-photon absorption cross sections and for two different values of $\tilde{\chi}_S^{(3)}(\omega)$. The strong solid curve corresponds to our Sr experiment. For each input intensity we searched for the optimum harmonic output by varying the column density, $N_0 L$, and the initial mismatch per number density, $\Delta k/N_0$. The resulting optimum values for these experimental parameters are shown in Fig. 6 and will be discussed below. From Fig. 5 we see that for low input intensities the harmonic intensity increases approximately with the third power of the input intensity and the conversion efficiency is inversely proportional to the square of the one-photon absorption cross section, in agreement with Eq. (24a). These calculations show that with decreasing one-photon absorption the harmonic intensity is limited to the value given by Eq. (29) due to the intensity-dependent mismatch. Increasing the input intensity above the saturation intensity [2.7×10^7 W/cm² for $\tilde{\chi}_S^{(3)}(\omega) = 2.13\times10^{-29}$ esu and 1.9×10^7 W/cm² for $\tilde{\chi}_S^{(3)}(\omega) = 4.26\times10^{-29}$ esu], one observes for $\sigma^{(1)}(3\omega) = 0$ a rapid increase in the maximum harmonic intensity, which finally, at very high input intensities, approaches the constant conversion efficiency given by Eq. (31).

In contrast to the case of no one-photon absorption, an upper limit for the harmonic intensity is observed for $\sigma^{(1)}(3\omega) \neq 0$ which depends on $\tilde{\chi}_S^{(3)}(\omega)$ and the value of $\sigma^{(1)}(3\omega)$. This upper limit results from the limitation in length imposed by the one-photon absorption coefficient (see Fig. 4).

The experimental parameters which give rise to the optimum harmonic output are plotted in Fig. 6. A discussion of these data can be separated into two parts.

(1) For input intensities well below the saturation intensity, $\Phi_0 \ll \Phi_S$, the one-photon absorption cross section has a strong influence on the optimum parameters. With increasing absorption cross section, the optimum column density $N_0 L$

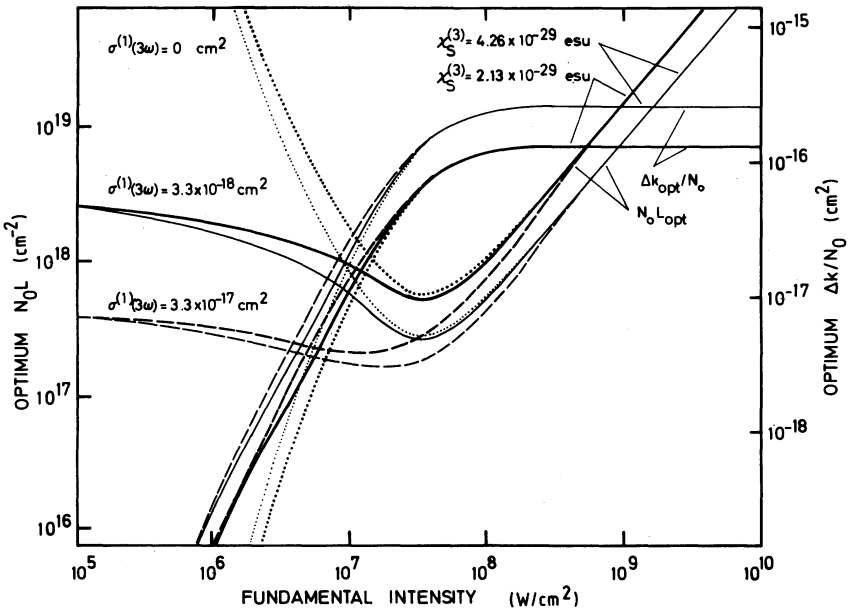

FIG. 6. Optimum column density $N_0 L$ and optimum normalized mismatch $\Delta k/N_0$ versus fundamental intensity for different values of the one-photon and two-photon absorption cross sections.

is reduced considerably down to an optical depth of $\sigma^{(1)}(3\omega)N_0L \simeq 5-10$. This results from a compromise between the one- and the two-photon absorption: Instead of reaching the optimum output at $N_0L \to \infty$, which is the case for negligible two-photon absorption, this additional nonlinear absorption gives rise to a finite optimum value for N_0L, according to Eq. (24a). The optimum initial mismatch is also influenced by the one-photon absorption, since with increasing cross section the effective interaction length is reduced (keeping the optical thickness constant) and hence a larger mismatch is allowed.

(2) For input intensities well above the saturation intensity $\Phi_0 \gg \Phi_S$, the optimum experimental parameters become independent of the one-photon absorption coefficient α_1, as the two-photon absorption coefficient α_2 exceeds α_1. With increasing input intensity the optimum value of N_0L increases and approaches the limit given by Eq. (32). This results from the bleaching of the nonlinear medium as the input intensity increases. At the same time, the optimum mismatch approaches the constant value of $\Delta k/N_0 = -(2\pi/c)^3 \times 3\omega(\tau_i \Delta\chi_i^{(1)})\tilde{\chi}_S^{(3)}(\omega)$, according to Eq. (27).

III. EXPERIMENTAL

The experimental arrangement consists of a flash-lamp-pumped dye laser tuned to the $5s^2$-$5s5d$ two-photon transition of Sr, a novel heat-pipe system for preparing the Sr-Xe mixture, and a diagnostic system for measuring the absolute intensity of the fundamental and the harmonic wave. The system is rather similar to the one previously described.[11] However, for testing the saturation phenomena predicted in Sec. II, two important modifications had to be made.

First of all, the column density of the Sr vapor was reduced in order to obtain an optically thin system. In this manner the phase-matching curve shows the typical periodic structure of an optically thin system and the important parameters of the nonlinear medium can be determined more accurately. In addition, the effects due to the one-photon absorption[11] can be distinguished more easily from the intensity-dependent effects which are of interest in this work. In order to handle short vapor columns with a well-defined length at vapor pressures near or even below the melting point of the active medium, the concentric heat-pipe oven[30] had to be modified in a manner to be described elsewhere.[31] In the experiments we used a length of the nonlinear medium of 5 cm and a Sr vapor pressure of 3.2 Torr ($N_0 = 2.87\times10^{16}$ cm^{-3}) corresponding to an optical depth of 0.5. The density gradient in the transition zones between the nonlinear medium and the confining noble gas was found to be identical with the gradient measured in the concentric heat-pipe oven.[11] However, the effect of the density gradient on the phase-matching curve is more pronounced because of the shorter length of the homogeneous nonlinear medium with respect to the transition zones.

As a further modification, the flash-lamp-pumped dye laser was followed by an inverted telescope. The purpose of this was to raise the beam intensity for the investigation of the saturation effects and to maintain a sufficiently parallel beam. A tightly focused beam had a severe effect on the phase-matching curve smearing out the periodic structure. The focusing of a multimode laser beam as it was used in our experiments leads to a rather complicated radial intensity distribution and it causes additional phase shifts[32] which obscure the influence of the intensity-dependent changes of the refractive index due to the two-photon absorption. Since the theory of the preceding section was not designed to describe a tightly focused multimode beam, the laser beam had to be carefully prepared with respect to its beam profile. For this reason the inverted telescope was adjusted at low input intensities in such a manner that the phase-matching curve shows the largest contrast between the maximum and the first minimum (see Fig. 7). This method turned out to be the most sensitive and reliable test of a parallel beam. However, due to the rather large beam divergence of 10^{-3} rad, the maximum achievable intensity of our laser system was limited to 1.3×10^7 W/cm^2.

In order to specify all the important nonlinear parameters which were not yet determined in our previous paper[11] and which are required for a test of the theory, the two-photon absorption cross section of the $5s^2$-$5s5d$ transition in Sr had to be measured. This was done by measuring the transmission of the vapor column as a function of the laser wavelength for different intensities and different particle densities. In this manner the value of $\tilde{\chi}_S^{(3)}(\omega)$ is obtained with a laser linewidth of 0.3 cm^{-1} according to Eqs. (6) and (15a). For this the beam radius, the density profile in the transition zones, and the length of the Sr vapor column have to be accurately known.

IV. RESULTS

For the investigation of the harmonic generation in nonlinear systems, the phase-matching curve holds the key to a detailed quantitative understanding of the different physical processes involved. The position of the minima and maxima is determined by the product of the length L and the mis-

match Δk of the nonlinear medium. The intensity ratio of the maxima and minima is a measure of the optical depth for the generated harmonic radiation and is also affected by the beam profile of the incident fundamental wave. The asymmetry of the phase-matching curve reveals the particle-density distribution along the optical path within the nonlinear medium.

We therefore started our experiments by recording phase-matching curves at different input intensities. Figure 7 shows two phase-matching curves taken with input intensities of 1.5×10^6 and 1.3×10^7 W/cm^2, respectively. The individual points represent an average of ten laser shots. Figure 7 also shows a typical error bar.

We first restrict our attention to the lower of the two phase-matching curves. The intensity of the incoming fundamental wave was attenuated to a level where the onset of saturation effects can certainly be neglected. Nevertheless, the phase-matching curve looks quite different from the one shown in Fig. 5 of Ref. 11. The width of the maximum which gives rise to the highest conversion efficiency, is significantly larger and shifted down to a smaller pressure ratio P_{Xe}/P_{Sr} corresponding to a higher value of Δk. Furthermore, the phase-matching curve shows a well-developed periodic structure on the low-pressure side. The different shape of the phase-matching curves is primarily due to the different optical depths. The measurements of Fig. 5 of Ref. 11 were taken with an optical depth of 7.5, whereas the optical depth in Fig. 7 amounts to 0.5. Besides lowering the particle density, the optical depth was mainly reduced by lowering the length of the nonlinear medium to 5 cm. Since the density profile of the transition zones between the nonlinear medium and the confining noble gas are identical for both sets of measurements, they have to play a more prominent role for the phase-matching curve in Fig. 7 where the length of the homogeneous section of the nonlinear medium is significantly shorter.

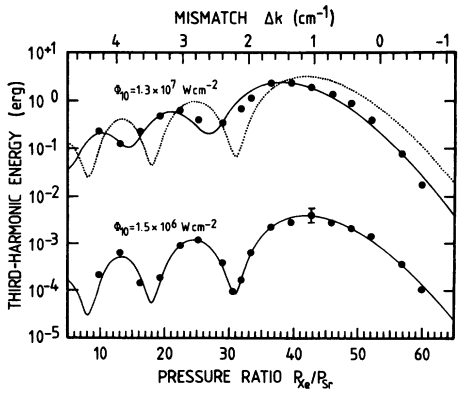

FIG. 7. Phase-matching curves of the Sr-Xe system taken with a parallel beam at two different input intensities. The solid lines represent theoretical curves. For the lower one, saturation effects due to two-photon absorption can be neglected, whereas for the upper phase-matching curve, saturation effects are important. The dotted line shows the calculations neglecting saturation effects.

The solid curve in Fig. 7 represents the theoretical phase-matching curve which is in excellent agreement with the experiments. For the lower one of the two curves, the linear and nonlinear susceptibilities and the density gradient were all taken from Ref. 11.

Increasing the input intensity to $\Phi_0 = 1.3\times10^7$ W/cm^2, one obtains the upper phase-matching curve in Fig. 7. Neglecting all the saturation effects due to intensity-dependent changes of the refractive index, the theoretical phase-matching curve would be given by the dotted line in Fig. 7 which differs quite dramatically from the measurements. If one, however, includes the intensity-dependent changes of the level populations associated with the two-photon absorption, the corresponding changes of the refractive index give rise to a theoretical phase-matching curve (upper solid line) which is again in excellent agreement with the experiments.

For the calculation of the upper phase-matching curve, the two-photon absorption cross section of the $5s^2$-$5s5d$ transition is required. It was measured independently as described in Sec. III and we obtained $\tilde{\chi}_S^{(3)}(\omega) = 4.3\times10^{-30}$ esu for a linewidth of 1 cm^{-1}. From this value the matrix element of the $5s5d$-$5s5p$ transition was extracted and used to calculate the linear susceptibilities of the $5s5d$ and $5s5p$ levels at the wavelengths of the fundamental and the third-harmonic wave.[29] With these parameters the upper phase-matching curve in Fig. 7 was calculated according to Eqs. (14) and (15). It is important to note that there is no free adjustable parameter.

There is another important piece of experimental evidence for the strong two-photon absorption. At high input intensities we noticed stimulated emission from the $5s5d$ state to the lower $5s5p$ state due to a population inversion originating from the two-photon excitation of the $5s5d$ state. For a quantitative agreement with the experiments, we had to incorporate this process in our calculations by modifying the set of rate equations (9). It was assumed that the population of the $5s5d$ state follows directly the population of the $5s5p$ state due to stimulated emission. As a result, taking into account the different statistical weights, the $5s5d$ state effectively adopts the lifetime of the $5s5p$ state which is well known.

Two significant féatures of the high-intensity

phase-matching curve are apparent from Fig. 7, namely a shift of the periodic structure to smaller pressure ratios and a reduced amplitude of the periodic structure. The shift is mainly due to the quantity $(\tau_i \Delta\chi_i^{(1)})$ defined in Eq. (19b). The reduced values of the maxima originate from the depletion of the fundamental wave due to the two-photon absorption and the corresponding lower population difference ΔN between the ground state and the two-photon resonant state of the nonlinear medium. The filling up of the minima is related to the temporal and radial intensity distribution of the incident laser pulse because the final phase-matching curve results from an integration in time and space where contributions of different parts of the beam give rise to different changes of the refractive index.

Finally, Fig. 8 shows the third-harmonic power as a function of the fundamental intensity for two different pressure ratios $P_{Xe}/P_{Sr} = 46.3$ (rectangular points) and 31.8 (circular points). The two values are on the high-pressure side and the low-pressure side of the phase-matching maximum in Fig. 7 and they were chosen in such a manner that they give the same conversion efficiency for an input intensity of 1.3×10^7 W/cm^2. Each point in Fig. 8 is again an average of ten laser shots. The solid lines give the theoretical curves and the dotted lines indicate a power law with a slope of 3.

The measurements in Fig. 8 clearly show the onset of the saturation and the influence of the initial mismatch as discussed in Sec. II. At low intensities both sets of measurements increase as the cube of the fundamental intensity. The harmonic power obtained with the higher pressure ratio exceeds the measurements taken with the lower pressure ratio by about one order of magnitude. With increasing fundamental intensity, the high-pressure curve starts to differ from the simple third-power law (dotted line) until it levels off around the saturation intensity Φ_S of 2.7×10^7 W/cm^2 due to the depletion of the fundamental wave and the bleaching of the nonlinear medium. The low-pressure curve, on the other hand, behaves quite differently. Here the change in the refractive index causes a dramatic increase of the generated third-harmonic power and around 10^7 W/cm^2, the low-pressure curve even overtakes the high-pressure curve. The theoretical curve then levels off at a third-harmonic power which is larger by one order of magnitude than the value of the high-pressure curve. This behavior clearly reveals the importance of the initial mismatch which improves the conversion efficiency at high input intensities, as explained in detail in Sec. II.

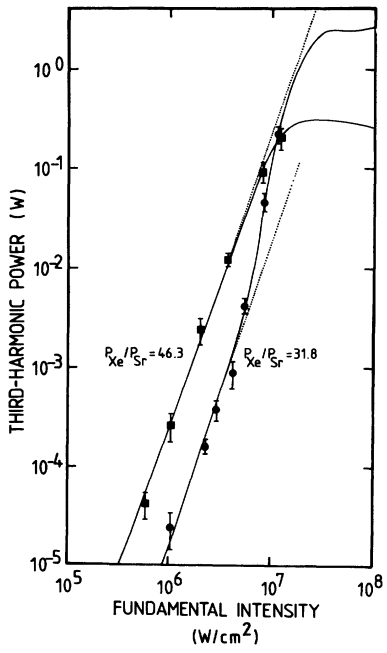

FIG. 8. Third-harmonic power versus fundamental intensity for two different pressure ratios P_{Xe}/P_{Sr}. The calculations are carried out including (solid lines) and neglecting (dotted lines) saturation effects due to two-photon absorption.

V. SUMMARY

A detailed quantitative analysis of the saturation of two-photon resonant THG in absorbing media has been presented. It includes the one-photon absorption of the third-harmonic wave as well as the two-photon absorption of the fundamental wave which gives rise to a depletion of the fundamental wave and a change of the population densities. The latter process is shown to lead to a change of the effective refractive index and is the limiting process in the conversion efficiency because of the destruction of the phase-matching condition.

For high-density systems the limiting processes occur at power levels where Stark shifts can still be neglected. The optimum conditions are presented and the importance of the one-photon absorption for low input intensities and of the two-photon absorption at high input intensities is demonstrated.

It is shown that for resonant THG in phase-matched systems, the highest achievable conversion efficiency is given by $\eta_{max} = |3\chi_T^{(3)}(3\omega)/\tilde{\chi}_S^{(3)}(\omega)|^2$. Consequently, for resonant as well as nonresonant THG, the limiting processes are due to the same nonlinear susceptibilities. The nonresonant case is governed by the real part of the nonlinear susceptibilities, whereas for resonant

systems the imaginary parts dominate. It should be noted that the limiting nonlinear susceptibilities $\chi_s^{(3)}$ are also resonantly enhanced. As a result, the advantage of resonant THG at low input intensities turns into a disadvantage at high input intensities and it explains why the highest conversion efficiencies achieved so far in nonresonant systems significantly exceed those obtained with resonant systems.

In addition to the theoretical analysis, measurements have been presented which demonstrate the onset of the saturation due to two-photon absorption and which are in excellent agreement with the theory.

ACKNOWLEDGMENT

It is a great pleasure to acknowledge the support given by the Deutsche Forschungsgemeinschaft.

---

*Present address: Kristalloptik Laserbau G.m.b.H. Am Sulzbogen 62, 8080 Fürstenfeldbruck, Germany.

[1]R. T. Hodgson, P. P. Sorokin, and J. J. Wynne, Phys. Rev. Lett. 32, 343 (1974).
[2]K. M. Leung, J. F. Ward, and B. J. Orr, Phys. Rev. A 9, 2440 (1974).
[3]C. C. Wang and L. I. Davis, Jr., Phys. Rev. Lett. 35, 650 (1975).
[4]J. F. Ward and A. V. Smith, Phys. Rev. Lett. 35, 653 (1975).
[5]S. C. Wallace and G. Zdasiuk, Appl. Phys. Lett. 28, 449 (1976).
[6]V. I. Anikin, S. A. Akhmanov, K. N. Drabovich, and A. N. Dubovik, Kvantovaya Elektron. (Moscow) 3, 2014 (1976) [Sov. J. Quantum Electron. 6, 1096 (1976)].
[7]J. R. Taylor, Opt. Commun. 18, 504 (1976).
[8]A. I. Ferguson and E. G. Arthurs, Phys. Lett. 58A, 298 (1976).
[9]D. I. Metchkov, V. M. Mitev, L. I. Pavlov, and K. V. Stamenov, Phys. Lett. 61A, 449 (1977).
[10]K. N. Drabovich, D. I. Metchkov, V. M. Mitev, L. I. Pavlov, and K. V. Stamenov, Opt. Commun. 20, 350 (1977).
[11]H. Scheingraber, H. Puell, and C. R. Vidal, Phys. Rev. A 18, 2585 (1978).
[12]D. M. Bloom, G. W. Bekkers, J. F. Young, and S. E. Harris, Appl. Phys. Lett. 26, 687 (1975).
[13]H. Puell, K. Spanner, W. Falkenstein, W. Kaiser, and C. R. Vidal, Phys. Rev. A 14, 2240 (1976).
[14]H. B. Puell and C. R. Vidal, IEEE J. Quantum Electron. QE-14, 364 (1978).
[15]J. C. Diels and A. T. Georges, Opt. Lett. 1, 158 (1977).
[16]J. N. Elgin and G. H. C. New, J. Phys. B 11, 3439 (1978).
[17]J. C. Diels and A. T. Georges, Phys. Rev. A 19, 1589 (1979).
[18]J. N. Elgin and G. H. C. New, Opt. Commun. 16, 242 (1976).
[19]A. T. Georges, P. Lambropoulos, and J. H. Marburger, Opt. Commun. 18, 509 (1976).
[20]A. T. Georges, P. Lambropoulos, and J. H. Marburger, Phys. Rev. A 15, 300 (1977).
[21]Two-component phase-matching was not possible in case of Ref. 4 since Cs shows normal dispersion when using ruby laser light as fundamental wave.
[22]J. N. Elgin, G. H. C. New, and K. E. Orkney, Opt. Commun. 18, 250 (1976).
[23]V. I. Anikin, V. D. Gora, K. N. Drabovich, and A. N. Dubovik, Kvantovaya Elektron. (Moscow) 3, 330 (1976) [Sov. J. Quantum Electron. 6, 174 (1976)].
[24]J. A. Armstrong, N. Bloembergen, J. Ducuing, and P. S. Pershan, Phys. Rev. 127, 198 (1962).
[25]H. Puell and C. R. Vidal, Phys. Rev. A 14, 2225 (1976).
[26]G. Peach, Mem. R. Astron. Soc. 71, 13 (1967).
[27]M. Abramowitz and I. A. Stegun, *Handbook of Mathematical Functions* (U.S. Nat. Bur. Stand. App. Math. Ser. No. 55, Washington, D.C., 1964).
[28]E. A. Stappaerts, IEEE J. Quantum Electron. QE-15, 110 (1979).
[29]H. Scheingraber, thesis, Technische Universität München, 1979 (unpublished).
[30]C. R. Vidal and F. B. Haller, Rev. Sci. Instrum. 42, 1779 (1971).
[31]H. Scheingraber and C. R. Vidal (unpublished).
[32]Yun Mui Yiu, T. J. McIlrath, and R. Mahon, Phys. Rev. A 20, 2470 (1979).